

Investigating Renewable Infeed in Residential Areas Applying Model Predictive Control

Michèle Arnold, *Student Member, IEEE*,
Göran Andersson, *Fellow, IEEE*

Abstract—The operation and optimization of integrated electricity and natural gas systems is investigated. The couplings between these different infrastructures are modeled by energy hubs, which can convert and store different types of energy. In previous work, the interaction between three interconnected hubs has been analyzed. In order to take into account predicted system behavior and operational constraints, a model predictive control approach is proposed for optimal operation. In this paper, the hubs, representing residential areas, are also connected to a grid. The energy exchange not only between hubs but also between hubs and the grid is investigated. The hubs contain solar PV installations wherewith they have the ability to feed in energy to the grid. Simulations are presented where the proposed scheme is applied to the hub system. Operational costs are compared for system operation with and without renewable infeed.

Index Terms—Power system optimization, model predictive control, multi-carrier energy systems, energy hub, nodal prices

I. INTRODUCTION

MOST of today's energy infrastructures evolved during the second part of the last century and are traditionally based on hierarchical electricity networks, where electricity is produced in centralized power plants with accordingly high production ratings. Within this scheme, energy obtained by centralized production on the higher voltage levels is transported and distributed to consumers on the lower voltage levels, resulting in unidirectional energy flows. However, the perspectives of an optimal operation of the power system have changed in the last years. The energy production changes more and more from centralized units to diverse distributed production units. Such units, e. g., photovoltaics, wind, micro combined heat and power plants (μ CHP), waste and wood incineration plants etc., can also be located at lower voltage levels. Furthermore, the installations of renewable energy resources are promoted by receiving a feed-in tariff to cover the high installation costs. Incentives for this trend are, amongst others, the desire to quit dependency on limited fossil energy resources, increased energy trading and exchange due to the on-going energy market liberalization and the increased social awareness to utilize more sustainable and environmentally friendly energy sources. The lower level distributed generation (DG) units are able to feed in energy at different locations and at different voltage levels, which leads to bidirectional power flows within the distribution as well as within the transmission network. This evolution complicates the operation of the

network, but at the same time provides opportunities for consumers and local energy production units.

Another changing aspect within the current power system structure is that energy supply is no longer based only on electricity networks, but other energy carrier networks, such as gas, hydrogen or local heating networks, must be taken into account as well. The utilization of DG units, so-called co- and tri-generation plants [1], which couple different types of infrastructures is increasing. For example, micro combined heat and power plants (μ CHP) produce simultaneously electricity and heat by consuming gas, therefore coupling electricity, gas and heat networks. This increasing coupling between the individual systems gives rise to pursue the integrated control of several of such systems. Due to the availability of the various energy carriers, consumers are more flexible in their purchasing and make decisions depending on criteria such as costs, reliability, system emissions or a combination of them.

In order to investigate these aspects an appropriate modeling framework of the energy network is needed. Several conceptual approaches for describing systems including DG units and various infrastructure systems have been examined. Besides "energy-services supply systems" [2], "basic units" [3], "micro grids" [4], and "virtual power plants" (VPP), so-called "energy hubs" [5] are proposed to address these kind of systems. The latter formulation has been established within the project "Vision of Future Energy Networks", which was initiated at ETH Zurich. The energy hub approach is a general modeling framework which allows to model the power system with respect to the aspects discussed above. Energy systems are considered to consist of a number of interconnected energy hubs, which represent the interface between the consumers and the power supply infrastructures of the different energy systems.

To determine the optimal operation of the multi-carrier energy system, an optimal power flow (OPF) problem is solved. Since storage devices with dynamic behavior are present in the considered system, an optimization over multiple time steps is necessary to handle the dependency between consecutive time steps. To optimize the operation over multiple time steps, we apply model predictive control (MPC) [6], [7], wherewith system dynamics, forecasts and operational constraints are taken into account explicitly. In our application, we use MPC to determine the actions for the individual energy hubs, which give the best predicted behavior, e.g., minimal energy costs, based on the characteristics of the energy supply infrastructures, the dynamics of the storage devices, and the load and price profiles. By using a predictive approach, the

M. Arnold (corresponding author) and G. Andersson are with the Power Systems Laboratory, ETH Zurich (Swiss Federal Institute of Technology), Physikstrasse 3, 8092 Zürich, Switzerland, e-mail: {arnold, andersson}@eeh.ee.ethz.ch.

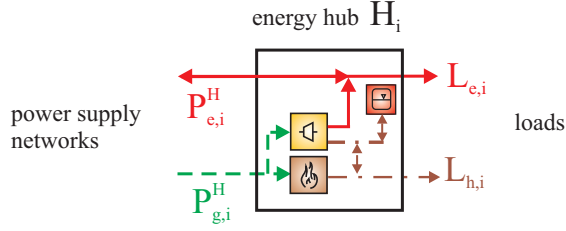


Fig. 1. Example of an energy hub containing a μ CHP device, furnace and heat storage. Hub is connected to electricity and natural gas power supply networks and supplies electrical and heat loads.

energy usage can be adapted to fluctuations of energy prices and of load and renewable input profiles.

The remainder of this paper is organized as follows. Section II presents the basic design concepts of energy hubs and how they are used in energy systems. The mathematical model of the considered hub system is given in Section III. Section IV presents the MPC control approach for the optimal operation of the system. Results of simulations applying the proposed approach to the hub system are presented in Section V. Section VI concludes this paper and outlines directions for future research.

II. SYSTEM DESIGN CONCEPTS

The basic concepts of the energy hub as a single unit and of energy systems considered as interconnected energy hubs are explained in the following subsections. Here, an integrated electricity and natural gas system is considered.

A. Hub Concept

Combining infrastructures means coupling them at certain nodes, thereby enabling exchange of power between previously separated systems. These couplings and interactions can be described by means of the energy hub, with which storage of different forms of energy and conversion between them can be formulated [5]. Figure 1 shows an exemplary energy hub H_i which consumes or delivers electricity $P_{e,i}^H$ and consumes natural gas $P_{g,i}^H$ at the input and supplies energy to electrical loads $L_{e,i}$ and heat loads $L_{h,i}$. The hub contains a μ CHP device and a furnace for energy conversion and a heat storage for energy storage. The electricity produced using the μ CHP can either be used to supply the electrical load or can be fed back to the grid (arrows). The heat produced, by both μ CHP and furnace, is used either to supply the heat load or to fill up the storage. If the produced heat is not sufficient to cover the heat demand, the storage is used for support. The coupling provided by the μ CHP device increases the redundancy in supply and offers the opportunity of optimizing the energy supply, e.g., supplying the electrical load via μ CHP which is particularly lucrative at high electricity import prices.

The energy hub concept enables the integration of an arbitrary number of energy carriers and products (such as conversion and storage units) and thus provides high flexibility in system modeling. Single power plants or industrial buildings

as well as bounded geographical areas, such as whole towns and cities, can be modeled as energy hubs.

B. Hubs in Energy Systems

The considered system (Fig. 2) consists of an integrated electricity and natural gas system, where the two systems are connected via energy hubs. This setup illustrates two hubs, structured as described above, connected to the supply grid. The hubs represent an aggregation of households. The gas pipeline network is modeled on a single pressure level. The electricity network covers both the low voltage level and the medium voltage level, as indicated with the transformers. The hubs H_1 and H_2 are connected to the low voltage level, e.g. 400 V, at buses 5 and 6, respectively. The aggregated households are assumed to have photovoltaics (PV) installed. These are modeled as renewable infeeds R_1 and R_2 at buses 5 and 6, respectively. Depending on the prices and loads, the produced solar electricity can be used either for supplying the own loads or can be fed back to the grid. On the higher voltage level (buses 1, 2 and 3), e.g., 16 kV, two local generators $P_{e,2}^G$ and $P_{e,3}^G$, which may be waste incineration plants or biomass processing units, are available for supplying the hub loads. The generator $P_{e,1}^G$, located at bus 4, e.g., 60 kV, represents the grid and is modeled as infinite bus with no generation or consumption restrictions. The gas supply is offered by an adjacent gas network N , where compressors (C_{ef} , for $(e, f) \in \{(1, 2), (1, 3)\}$) within the pipelines enable the gas flow to the hubs. Metering devices are installed to measure the energy consumption of the hubs. Two different methods for measuring the consumed energy, which will be discussed in more detail in section V-C, are indicated.

This system setup takes into account the increased penetration of distributed generation (μ CHP and local generators) and of renewable infeed (PV). Each household, or hub respectively, decides autonomously when to produce electricity locally via μ CHP, when to feed energy back to the grid and when to consume energy from higher network levels. The traditional power system model, where electricity generated with centralized units flows to the consumers' level, evolves to a model with active network nodes where consumers play an important role in optimizing the operation of the system.

III. MODELING

In this section, the mathematical model of the system setup introduced above is described. The equations for power conversion and power storage within the energy hubs, and for power transmission between the hubs are formulated. The equations are defined for time step k as we consider the optimal operation over multiple time steps. A discrete time step k corresponds to the continuous time kT , where T is one hour.

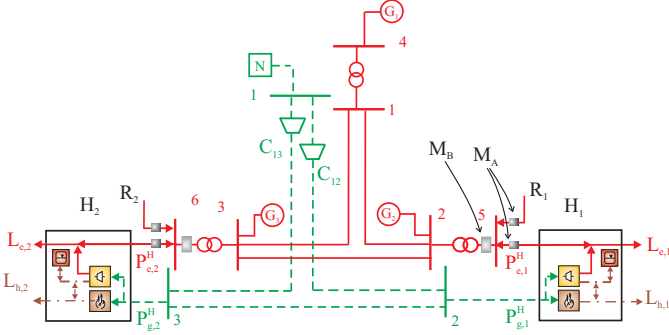


Fig. 2. System setup of two energy hubs connected to the supply grid. Active power is provided by generators G_1 , G_2 , G_3 , natural gas by the adjacent natural gas network N . Both hubs have a renewable infeed R_1 and R_2 .

A. Energy Hub

For both hubs H_i depicted in Fig. 1 the outputs $L_i(k) + M_i(k)$ and inputs $P_i(k)$ correlate as follows [5], [8]:

$$\underbrace{\begin{bmatrix} L_{e,i}(k) \\ L_{h,i}(k) + M_{h,i}(k) \end{bmatrix}}_{L_i(k) + M_i(k)} = \underbrace{\begin{bmatrix} c_{ee,i} & c_{ge,i} \\ c_{eh,i} & c_{gh,i} \end{bmatrix}}_{C_i(k)} \underbrace{\begin{bmatrix} P_{e,i}^H(k) \\ P_{g,i}^H(k) \end{bmatrix}}_{P_i(k)}, \quad (1)$$

where the electrical load $L_{e,i}(k)$ and the heat load $L_{h,i}(k)$ combined with the heat storage flow $M_{h,i}(k)$ are supplied by the electricity $P_{e,i}^H(k)$ and gas hub input $P_{g,i}^H(k)$. For this, the appropriate conversion between energy carriers is defined by the coupling matrix $C_i(k)$:

$$C_i(k) = \begin{bmatrix} 1 & \nu_{g,i}(k)\eta_{ge,i}^{\text{CHP}} \\ 0 & \nu_{g,i}(k)\eta_{gh,i}^{\text{CHP}} + (1 - \nu_{g,i}(k))\eta_{gh,i}^{\text{F}} \end{bmatrix}. \quad (2)$$

The elements of the coupling matrix are composed of converter efficiencies η and dispatch factors ν . The efficiencies of the μCHP device are defined by $\eta_{ge,i}^{\text{CHP}}$ (gas-electric) and $\eta_{gh,i}^{\text{CHP}}$ (gas-heat), the efficiency of the furnace is given by $\eta_{gh,i}^{\text{F}}$ (gas-heat). In cases where an input, such as the gas input $P_{g,i}^H$, is diverted to multiple converter devices, a dispatch factor $\nu_{g,i}(k)$ ($0 \leq \nu_{g,i}(k) \leq 1$) determines how the gas is divided between the μCHP and the furnace. As the dispatch factor $\nu_{g,i}(k)$ is a control variable, different input vectors can be found to fulfill the output requirements. This reflects the degrees of freedom in supply which are used for optimization.

Apart from conversion units there is a heat storage present. It is modeled as an ideal storage unit in combination with a storage interface [5]. The thermal power exchange $M_{h,i}(k)$ is defined as the difference between the actually stored energy $E_{h,i}(k)$ at two consecutive time steps, plus some standby energy losses $\dot{E}_{\alpha,i}^{\text{stb}}$ which must be covered at each time period ($\dot{E}_{\alpha,i}^{\text{stb}} \geq 0$):

$$\begin{aligned} M_{h,i}(k) &= \frac{\dot{E}_h}{e_{h,i}} = \frac{1}{e_{h,i}} \frac{dE_{h,i}}{dt} \approx \frac{1}{e_{h,i}} \frac{\Delta E_{h,i}}{\Delta t} \\ &= \frac{1}{e_{h,i}} \left(\frac{E_{h,i}(k) - E_{h,i}(k-1)}{\Delta t} + \dot{E}_{h,i}^{\text{stb}} \right). \end{aligned} \quad (3)$$

B. Energy Transmission Network

As described above, electricity networks and gas pipeline networks serve as interconnecting energy transmission networks. Both are modeled by power flow equations: nodal power balances of the complex power are formulated for the AC electricity network [9], [8], nodal volume flow balances are defined for the pipeline network [8]. The gas pipeline is modeled as being composed of a compressor with pressure amplification p_{inc} and a pipeline element. The transformers are modeled as ideal transformer with a series reactance [9]. For a more detailed description of the energy transmission networks, see [8].

IV. CONTROL

For the optimal operation of the system introduced above a centralized, supervisory controller which measures all variables and determines all actuator settings is implemented. The goal of the controller is to determine control variables $\mathbf{u}(k)$ in such a way that the total operational costs of the system are minimized while satisfying the system constraints. In order to appropriately take the dynamics of the storage devices and the characteristics of the electricity and gas networks into account, we propose a model predictive control (MPC) approach. Next, we shortly explain the basic idea of MPC, then the control problem for the introduced system setup is formulated and finally the derivation of the nodal prices as outcome of the optimization is explained.

A. Model Predictive Control

Model Predictive Control (MPC) [6],[7] is a control strategy which uses an internal prediction model to find those actions that give the best predicted system behavior over a certain prediction horizon with length N . MPC operates in a receding horizon manner, i.e. at each time step new measurements of the system and new predictions into the future are made. By using MPC, actions can be determined that anticipate future events and changes, such as increasing or decreasing energy prices.

Figure 3 illustrates the procedure schematically. At each discrete control step k , the MPC controller determines the control settings $\tilde{\mathbf{u}}(k)$ that give, according to the given objective function, the best predicted performance of the system for the next N time steps. The tilde over the variable represents that variable over the whole prediction horizon of N steps, i.e. $\tilde{\mathbf{u}}(k) = [\mathbf{u}^T(k), \dots, \mathbf{u}^T(k+N-1)]^T$. The control variables for the current time step k , $\mathbf{u}(k)$, are then applied to the system. The system proceeds to a new state, $\mathbf{x}(k+1)$, where the whole cycle is repeated with updated system measurements.

B. Problem Formulation

For the system under consideration, the control objective is to minimize the energy costs for electricity and natural gas consumption:

$$J = \sum_{l=0}^{N-1} \sum_{i_G=1}^3 q_{i_G}^G(k+l)(P_{e,i_G}^G(k+l))^2 + q^N(k+l)P_g^G(k+l), \quad (4)$$

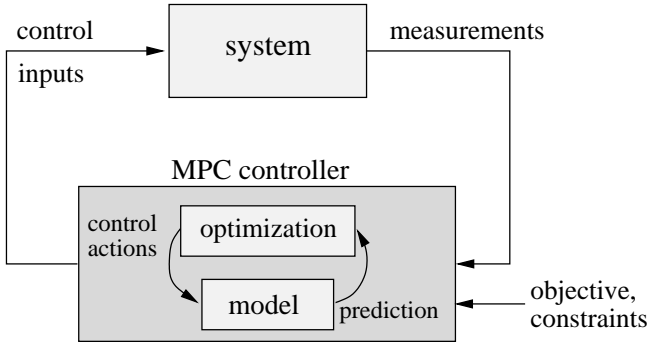


Fig. 3. Illustration of model predictive control, showing interactions between system and controller.

where i_G indicates the generator and $q_{i_G}^G$ and q^N define the time varying prices for electricity generation (modeled as quadratic functions) and natural gas consumption (modeled as linear functions). This objective is minimized by determining the optimal operational set-points of the system:

$$\mathbf{u}(k) = [(\mathbf{P}_e^G)^T(k) \quad P_g^G(k) \quad \boldsymbol{\nu}_g^T(k)]^T, \quad (5)$$

where

- $\mathbf{P}_e^G(k) = [P_{e,1}^G(k), P_{e,2}^G(k), P_{e,3}^G(k)]^T$ denotes the active power generation of all generators,
- $P_g^G(k)$ defines the natural gas import and
- $\boldsymbol{\nu}_g(k) = [\nu_{g,1}(k), \nu_{g,2}(k)]^T$ describes the dispatch factors at the gas input junctions.

The overall control problem is finally stated as

$$\min_{\tilde{\mathbf{u}}(k)} J(\tilde{\mathbf{x}}(k+1), \tilde{\mathbf{z}}(k), \tilde{\mathbf{u}}(k)) \quad (6)$$

subject to

$$\tilde{\mathbf{x}}(k+1) = \tilde{\mathbf{f}}(\tilde{\mathbf{x}}(k), \tilde{\mathbf{z}}(k), \tilde{\mathbf{u}}(k)) \quad (7)$$

$$\tilde{\mathbf{g}}(\tilde{\mathbf{x}}(k), \tilde{\mathbf{z}}(k), \tilde{\mathbf{u}}(k)) = \mathbf{0} \quad (8)$$

$$\tilde{\mathbf{h}}(\tilde{\mathbf{x}}(k), \tilde{\mathbf{z}}(k), \tilde{\mathbf{u}}(k)) \leq \mathbf{0}. \quad (9)$$

In addition to the control variables $\mathbf{u}(k)$, an algebraic state vector $\mathbf{z}(k)$ and a dynamic state vector $\mathbf{x}(k)$ occur in the optimization problem. The dynamic state vector includes variables for which dynamics are explicitly defined, i.e. the energy contents of the storage devices. The algebraic state vector includes variables with no dynamics defined:

$$\mathbf{x}(k) = [\mathbf{E}_h(k)]^T \quad (10)$$

$$\mathbf{z}(k) = [\mathbf{V}^T(k) \quad \boldsymbol{\theta}^T(k) \quad \mathbf{p}^T(k) \quad \mathbf{p}_{\text{inc}}^T(k) \quad (\mathbf{P}_e^H)^T(k) \quad (\mathbf{P}_g^H)^T(k)]^T \quad (11)$$

where

- $\mathbf{V}(k) = [V_1(k), V_2(k), V_3(k), V_4(k), V_5(k), V_6(k)]^T$ and $\boldsymbol{\theta}(k) = [\theta_1(k), \theta_2(k), \theta_3(k), \theta_4(k), \theta_5(k), \theta_6(k)]^T$ denote the voltage magnitudes and angles of the electric buses, respectively,
- $\mathbf{p}(k) = [p_1(k), p_2(k), p_3(k)]^T$ denotes the nodal pressures of all gas buses,
- $\mathbf{p}_{\text{inc}}(k) = [p_{\text{inc},1}(k), p_{\text{inc},2}(k)]^T$ denotes the pressure amplification of the compressors,

- $\mathbf{P}_e^H(k) = [P_{e,1}^H(k), P_{e,2}^H(k)]^T$ denotes the electric inputs of the hubs,
- $\mathbf{P}_g^H(k) = [P_{g,1}^H(k), P_{g,2}^H(k)]^T$ denotes the gas inputs of the hubs and
- $\mathbf{E}_h(k) = [\mathbf{E}_{h,1}(k), \mathbf{E}_{h,2}(k)]^T$ denotes the energy contents of the heat storage devices.

Equation (7) represents the difference equations of the storage devices. The equalities (8) summarize all power flow equations of the electricity and gas networks as well as the hub equations. The inequality constraints (9) comprise limits on the voltage magnitudes, pressures, changes in compressor settings, dispatch factors, power limitations on hub inputs and limits on storage contents and storage flows.

The optimization problem (6)–(9) is a nonlinear programming problem [10]. In general, the solution space is non-convex and therefore finding the global optimum cannot be guaranteed applying numerical methods.

C. Nodal Prices

For each of the hubs we want to investigate the operation costs that appear within the simulation period. For this, the nodal prices or locational marginal prices (LMP) for the electricity and gas system have to be determined. These are obtained by applying the KKT optimality conditions [11]. It should be noted that these conditions are, strictly speaking, only valid for convex optimization problems. However, we assume a convex subspace at the optimum, which as stated above is not necessarily a global optimum. The Lagrange function for the optimization problem (6) - (9) is stated as

$$\mathcal{L} = J(\mathbf{P}) + \lambda \mathbf{g}_P(\mathbf{P}) + \mu \mathbf{h}_P(\mathbf{P}), \quad (12)$$

where $\mathbf{P} \in \{P_{e,i}^G, P_g^G\}$ and \mathbf{g}_P and \mathbf{h}_P denote all equalities and inequalities which are dependent on \mathbf{P} , i.e. the power flow and volume flow equations of all nodes of the electricity and gas network, and the operational limits (e.g. line capacity limits), respectively. The first KKT condition requires that all partial derivatives of the Lagrange function with respect to the optimization variables are zero:

$$\frac{\partial \mathcal{L}}{\partial \mathbf{P}} = \frac{\partial J(\mathbf{P})}{\partial \mathbf{P}} - \lambda - \mu \stackrel{!}{=} \mathbf{0} \quad (13)$$

$$\lambda = \frac{\partial J}{\partial \mathbf{P}} - \mu \quad (14)$$

The Lagrange multipliers λ correspond to the marginal cost or marginal benefit of power generation at that bus and some cost term for hit operational limits, such as congestion [12]. Assuming that there are no active inequalities, i.e. no hit operation limits, the μ term is zero. In this case we identify the nodal prices π as marginal costs of the respective energy carrier at a bus.

$$\pi = \lambda = \frac{\partial J}{\partial \mathbf{P}} \quad (15)$$

V. CASE STUDIES

The proposed control scheme is applied to the system depicted in Fig. 2. Firstly, the control variables and occurring operation costs are presented and secondly, the system

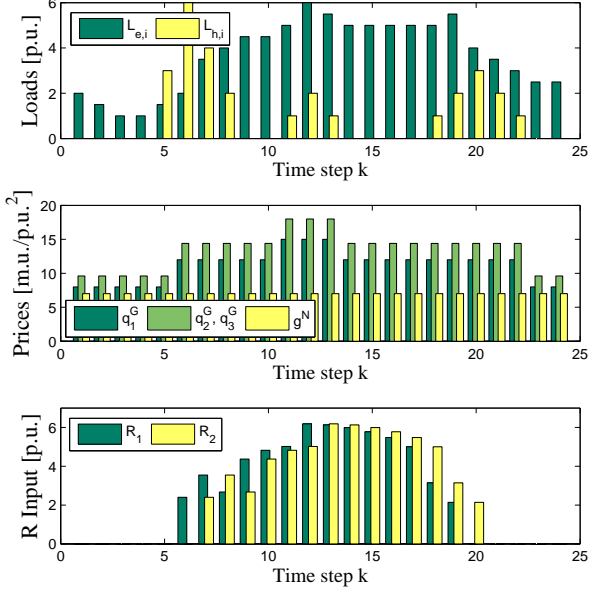


Fig. 4. Daily profile for electrical $L_{e,i}$ and heat loads $L_{h,i}$ (upper plot), prices for electricity q_{iG}^G and natural gas consumption q^N (central plot), and renewable infeed R_i (lower plot).

operation with and without renewable infeed is compared. To solve the optimization problems, the solver `snopt` through the Tomlab interface [13] in Matlab is used.

A. Simulation Setup

Each hub has a daily profile of load demands, energy prices and renewable inputs. Here, we assume these forecasts to be perfect, which is an idealization. However, it is believed that the following results are representative even in the presence of small forecast errors. The electrical and heat load profiles (Fig. 4, upper plot) are standardized profiles of a household, obtained by aggregating several households. The electricity prices vary during the day, showing a peak around noon, while gas prices are assumed to be constant during the day. For both hubs there exist renewable infeeds which are obtained by PV installations within the hub area, i.e. within the household aggregation. At hub H_1 , the solar production starts one hour earlier than for hub H_2 ¹. The loads and renewable infeeds are given in p.u. (per unit) values and the price coefficients are described in m.u./p.u.^2 for electricity and in m.u./p.u. for gas consumption, where m.u. refers to monetary units.

Regarding the electricity network, bus 4 is modeled as slack bus, i.e. having a fixed voltage angle and voltage magnitude ($V_4(k) = 1 \angle 0^\circ$ p.u.). Generator G_1 represents the grid, which can deliver and consume (unlimited) active power to and from the hub network. Buses 2 and 3 are PV buses, with specified voltage magnitude and net active power. Buses 1, 5 and 6 are modeled as PQ buses, with specified net active and reactive power. Regarding the gas network, bus 1 serves as slack bus,

¹These renewable input curves were obtained from solar measurements at Mont Soleil, Switzerland.

having a fixed pressure value of 1 p.u. Further details about the coefficients and simulation parameters used can be found in [8].

B. Control Variables

Based on the profiles specified above the total operation costs are minimized for a simulation of $N_{\text{sim}} = 24$ time steps, where one time step corresponds to 1 hour. The length of the prediction horizon N can be varied between $N=1$, i.e. no prediction, and $N = 24$, i.e. making a prediction for all 24 time steps. Choosing the prediction horizon length N is a trade-off between control performance on the one hand and computational effort on the other hand. For this application, we consider a prediction horizon length of $N = 3$ to be adequate. Accordingly, an optimization for 3 time steps is run, at each time step k implementing the control variables for the actual time step k , proceeding to the next time step $k + 1$ and starting the procedure again with updated system measurements. Running this scheme for the entire simulation period [1 ... 24], total operation costs of $1.4688 \cdot 10^3$ m.u. are obtained.

In Fig. 5 the evolution of the active power generation of all generators and the natural gas import is shown. The active power generation evolves proportionally to the difference between electrical load and renewable infeed, i.e. $\sim (L_{e,i} - R_i)$. Around noon, the amount of solar power is sufficient to supply the electrical load and some electric energy can even be exported, which is indicated by the negative value of generator G_1 . The natural gas import evolves similarly to the heat loads. Apart from supplying the heat loads, gas is also used for covering the heat storage standby losses, for filling up the storage devices before the heat load peaks and for supporting the expensive electricity consumption. At time steps where no heat is required, or no solar energy is available, (time steps 1–2 and 19–24), all gas is diverted to the μCHP device since electricity gained internally via μCHP is cheaper than by direct import from the grid. The heat thereby produced is stored and later used as heat supply. During the remaining time, the electricity system is not dependent on the gas network, since the renewable input is available "for free" during operation. In fact, this additional renewable infeed decouples the two systems. This decoupling is also visible in the behavior of the storage contents (see subsection V-D).

In Fig. 6, the net imported and exported amount of electric power for both hubs is shown. The imported and exported power corresponds to the difference between hub input and renewable input:

$$P_i^{\text{imp/exp}}(k) = P_{e,i}^H(k) - R_i(k). \quad (16)$$

Since the solar infeed at hub H_1 starts one hour earlier, hub H_1 starts to export earlier and also earlier to import again. At time step 6, the renewable infeed R_1 at hub H_1 exceeds the electrical load demand $L_{e,1}$, and therefore hub H_1 can export some electric energy in the morning.

C. Hub Operation Costs

As derived in section IV the nodal prices of all electricity and gas buses are directly obtained by solving the optimization

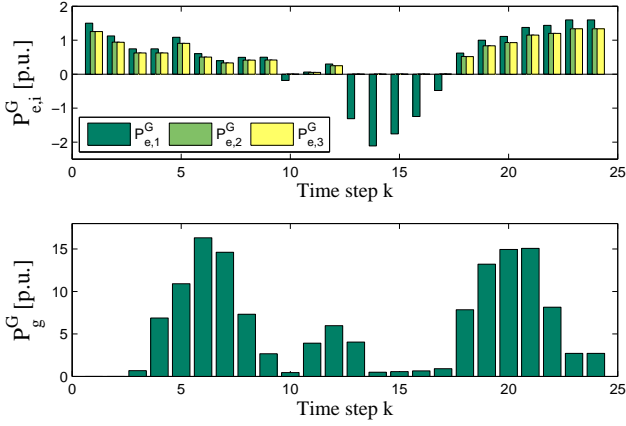


Fig. 5. Active power generation $P_{e,i}^G$ of all generators (upper plot) and natural gas import P_g^G (lower plot).

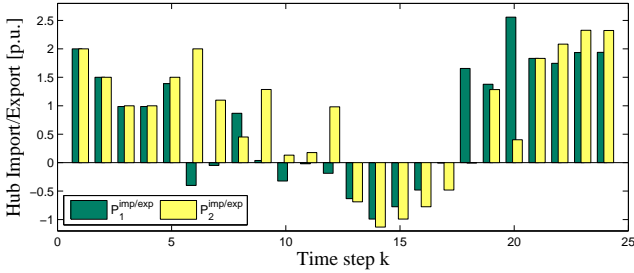


Fig. 6. Imported and exported electric power for hub H_1 (green bars) and hub H_2 (yellow bars).

problem (6)–(9). Figure 7 shows the evolution of all nodal prices over the entire simulation period. The nodal prices at all electricity buses n are almost the same, because only small losses occur on the lines (up to 0.4 %) and moreover because the generator prices are modeled as quadratic functions. The nodal prices (dashed line) evolve according to the imported amount of electric power, i.e. $P_i^{\text{imp/exp}} = P_{e,i}^H - R_i$, and become zero during exporting periods, i.e. when the renewable infeed is equal to or higher than the required load. This is due to the purely quadratic modeling of the electricity generation costs. If no active power is generated, nodal prices become zero because the marginal prices are linearly dependent on the amount of energy produced. The chain-dotted line represents the constant feed-in tariff c_i^R for solar energy. The feed-in tariff is assumed to be the same for both hubs, with a constant value of 3.5 p.u. The value of this feed-in tariff is dependent on the technology and on bilateral contracts with the energy suppliers. Contrary to the electricity system, the nodal prices of the gas system are different at each bus (solid lines). Losses within the gas pipelines, mainly compressor losses, are considerably higher (up to 28 %). Furthermore, gas prices are modeled as linear functions which implies larger differences between the nodal prices due to the constant part within the marginal costs. The nodal prices at bus 3 are higher than at bus 2 since losses on line 1-2 are higher than on line 1-3.

Next, we observe the operation costs that occur for each

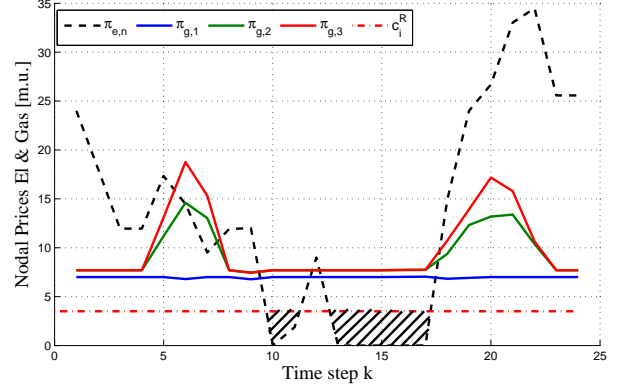


Fig. 7. Nodal prices for electricity buses (dashed line) and for gas buses (solid lines). Constant feed-in tariff for solar energy (chain-dotted line).

of the hubs. Thereby, we distinguish two models how to determine the costs regarding the consumed electricity. In Fig. 2 the installed metering devices are marked for both models. The subscript n refers to the corresponding node, where hub H_i is connected to, i.e. $n \in \{5,6\}$.

M_A : *feed-in tariff*: Two meters, which measure the the renewable infeed and the hub input, are installed. This measurement setting corresponds to the compensation principle that is used in many European countries, such as in Germany and Switzerland, for promoting installation of renewable energy generation. The resulting hub costs at every time step k are stated as

$$C_A^H(k) = \pi_{e,n}(k) \cdot P_{e,i}^H(k) - c_i^R \cdot R_i(k) + \pi_{g,n}(k) \cdot P_{g,i}^H(k). \quad (17)$$

M_B : *self-supply*: In this model only one meter, which measures the net imported or exported amount of electric energy, is installed. In this model, the ability of self-supply ranks first. Only the net amount of imported/ exported energy is charged, independently of the amount of actually produced energy with renewables. The hub are formulated as

$$C_B^H(k) = \pi_{e,n}(k)(P_{e,i}^H(k) - R_i(k)) + \pi_{g,n}(k) \cdot P_{g,i}^H(k). \quad (18)$$

Figure 8 shows the resulting hub costs of hub H_1 for cost models M_A and M_B , respectively. When comparing the models one notices above all a difference at those time periods, where the hubs are able to supply themselves or are even exporting electric energy, i.e. time steps 10 - 17. In Model M_A , the hub costs are negative, i.e. the hub makes some profit from selling renewable energy. When the nodal price is zero, meaning the hub input energy is "for free", the negative costs are the revenues for the solar energy. The peak at $k = 12$ arises from the peak in the nodal price (Fig.7), which again arises from the electricity load peak at noon (Fig.4). This peak does not occur in cost model M_B . In this model, the hub pays for the amount of imported energy and therefore the resulting costs remain positive. The negative peak at $k = 6$ arises because hub H_1 can export energy (Fig. 6) at a non-zero nodal price.

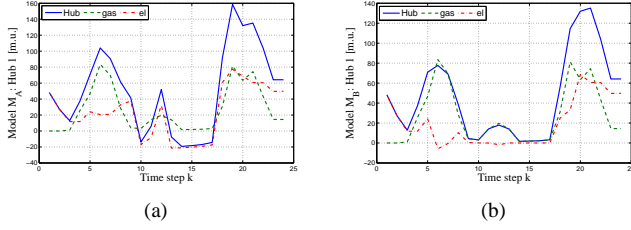


Fig. 8. Hub 1: Hub costs (solid line), gas costs (dashed line) and electricity costs (chain-dotted line) for (a) Model M_A , (b) Model M_B .

TABLE I
COMPARISON OF OPERATION COSTS, $m.u. \cdot 10^3$

$R/Model$	R, M_A	R, M_B	R, M_A	R, M_A	no R
Hub 1	1.21	1.11	1.43	1.11	5.76
Hub 2	1.31	1.17	1.53	1.17	5.98
c_i^R	[3.5,3.5]	-	[0,0]	[5.05,5.73]	-

The measuring method for the gas import does not change between the two cost models and therefore the same cost curves result for the gas import. Although the hub can profit from some revenues in model M_B , the overall costs for the entire simulation period are still higher. The feed-in tariff, chosen in this simulation, is mostly lower than the nodal price. Only during the marked area, model M_A is more profitable than model M_B . This changes of course when augmenting the feed-in tariff. The evolution of the cost curves for hub H_2 are similar to those of hub H_1 . The nodal prices at gas bus 3 are higher than at bus 2 which results in higher gas consumption costs for hub H_2 .

The hub costs summarized over the entire day for different feed-in tariffs are presented in Table I. The first two columns represent the two cases discussed above. In the third column, the renewable infeed is not refunded at all, $c_i^R = [0, 0]$, resulting in higher operation costs. In the fourth column the feed-in tariff is defined such that the costs for model M_A are the same as for model M_B . This is the case when refunding the renewable energy at a tariff of $c_i^R = [5.05, 5.73]$ m.u. Hub H_2 needs a higher feed-in tariff than hub H_1 in order to compensate for the higher amount of electrical input at hub H_2 . Because nodal gas prices are higher at hub H_2 than at hub H_1 , Hub H_2 consumes more electricity. The last entry in the table shows the costs when no renewable infeed is available. As expected, operation costs are considerably higher.

D. System Operation with/without Renewable Infeed

This subsection more precisely distinguishes the two cases of operation: with and without renewable infeed. The system operation without renewable infeed does, not only, cause higher operation costs but also influences the coupling between the electricity and natural gas system. In the case with no renewable infeed available, more gas is consumed, as electricity generated via μ CHP becomes cheap compared with the direct electricity import from the network. Accordingly, the μ CHP is in full operation during all time steps, except in the morning where the gas-heat capacity cannot cover the high heat load peak in the morning. At the same time the optimal

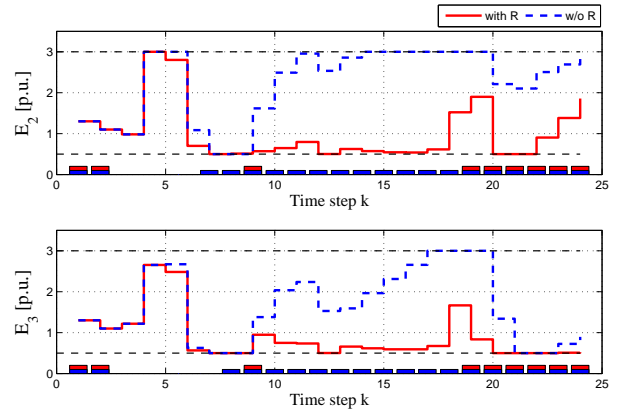


Fig. 9. Storage contents for system operation with renewable infeed (solid line) and without renewable infeed (dashed lines). μ CHP in usage with renewable infeed (red bars) and without renewable infeed (blue bars).

operation of the storage devices becomes more important. To optimize costs, the μ CHP device is operated as much as possible according to the electrical load. For this, the storage devices have to be filled up for supplying required heat loads as good as possible.

Figure 9 shows the storage contents for the system operation with renewable infeed (solid lines) and without renewable infeed (dashed lines). The bars at the bottom indicate when the μ CHP devices is in operation ($\nu_{g,i} \geq 0.5$, bar) and when not ($\nu_{g,i} \leq 0.5$, no bar). If no renewable input is available, heat storages are filled up before the heat load peaks and are emptied during the heat loads. In the case of a renewable input, the storage devices are filled up only rarely, for the noon heat load peaks almost not at all.

When minimizing the energy costs for the entire simulation period, total operation costs of $5.9621 \cdot 10^3$ m.u. result, compared to $1.4688 \cdot 10^3$ m.u. for the case with renewable infeed. Comparing the evolution of these operation costs over the time steps, one sees that the cost curve evolves proportional to the natural gas import in the case with renewable infeed and proportional to the sum of active power generation in the case without renewable infeed. In either case, the more expensive energy carrier determines the evolution of the costs, both for the net costs as well as for the hub costs.

VI. CONCLUSIONS AND FUTURE RESEARCH

We have presented the application of model predictive control to interconnected hub systems and have analyzed the interactions between hubs and the connected network. Moreover, the effects of renewable infeed in residential areas on overall system operation have been investigated. Integrating renewable energy decreases the peak loads and thus positively affects operational costs and operational limits. However, renewable infeed causes a decoupling between the two energy carriers for the considered system setup. Further research will address the incorporation of electric storage devices, since the effects of renewable electricity infeed are even more pronounced including electric storage devices. In addition, the system operation will be compared with the case where the centralized controller is replaced with a distributed controller.

ACKNOWLEDGMENTS

This research was supported by the project “Vision of Future Energy Networks” (VoFEN) of ABB, Areva T&D, Siemens, and the Swiss Federal Office of Energy. The authors would like to thank all colleagues of the Power systems laboratory (PSL) and M. Geidl from Swissgrid for the fruitful discussions.

REFERENCES

- [1] G. Chicco and P. Mancarella, “A comprehensive approach to the characterization of trigeneration systems,” in *Proc. of 6th World Energy System conference*, Turin, Italy, 2006.
- [2] H. M. Groscurth, T. Bruckner, and R. Kümmel, “Modeling of energy services supply systems,” *Energy*, vol. 20, no. 9, pp. 941–958, Jan. 1995.
- [3] I. Bouwmans and K. Hemmes, “Optimising energy systems, Hydrogen and distributed generation,” in *Proceedings of the 2nd International Symposium on Distributed Generation: Power System Market Aspects*, Stockholm, Sweden, Oct. 2002, pp. 1–7.
- [4] R. H. Lasseter and P. Piagi, “Microgrid: A conceptual solution,” in *Proceedings of the IEEE 35th Annual Power Electronics Specialists Conference*, Aachen, Germany, Jun. 2004, pp. 4285–4290.
- [5] M. Geidl and G. Andersson, “Optimal power flow of multiple energy carriers,” *IEEE Transactions on Power Systems*, vol. 22, no. 1, pp. 145–155, 2007.
- [6] J. M. Maciejowski, *Predictive Control with Constraints*. Harlow, England: Prentice Hall, 2002.
- [7] E. F. Camacho and C. Bordons, *Model Predictive Control*. New York, New York: Springer-Verlag, 2004.
- [8] M. Arnold, R. R. Negenborn, G. Andersson, and B. De Schutter, “Model-based predictive control applied to multi-carrier energy systems,” presented at the *IEEE PES General Meeting 2009*, Calgary, Canada, 2009.
- [9] P. Kundur, *Power System Stability and Control*. New York, New York: McGraw-Hill, 1994.
- [10] D. P. Bertsekas, *Nonlinear Programming*. Belmont, Massachusetts: Athena Scientific, 2003.
- [11] L. Chen, H. Suzuki, T. Wachi, and Y. Shimura, “Components of nodal prices for electric power systems,” *Proceedings of the IEEE Transactions on Power Systems*, vol. 17, no. 1, pp. 41–49, Feb. 2002.
- [12] A. J. Wood and B. F. Wollenberg, *Power Generation Operation and Control*, New York: John Wiley & Sons, Inc., 1996.
- [13] P. E. Gill, W. Murray, and M. A. Saunders, “SNOPT: An SQP algorithm for large-scale constrained optimization,” *SIAM Journal on Optimization*, vol. 12, no. 4, pp. 979–1006, 2002.



Michèle Arnold (S'07) was born in Bern, Switzerland. She received her MSc degree in electrical engineering and information technology from ETH Zurich (Swiss Federal Institute of Technology Zurich), Switzerland, in 2006.

In 2006, she joined the Power Systems Laboratory of ETH Zurich where she is working towards her PhD. Her research interests are modeling and optimization of power systems, multi-agent systems and distributed control.

She is a student member of IEEE.



Göran Andersson (M'86, SM'91, F'97) was born in Malmö, Sweden. He obtained his MSc and PhD degree from the University of Lund in 1975 and 1980, respectively.

In 1980 he joined ASEA, now ABB, HVDC division in Ludvika, Sweden, and in 1986 he was appointed full professor in electric power systems at the Royal Institute of Technology (KTH), Stockholm, Sweden. Since 2000 he is a full professor in electric power systems at ETH Zurich (Swiss Federal Institute of Technology Zurich), Switzerland. His research interests are in power system analysis, simulation and control. Another research interest is future energy and power systems.

He is a member of the Royal Swedish Academy of Engineering Sciences and Royal Swedish Academy of Sciences, and he is active in IEEE PES. He was the recipient of the IEEE PES Outstanding Power Educator Award 2007.